Concept of the solar ring mission: Overview

YuMing WANG, HaiSheng JI, YaMin WANG, LiDong XIA, ChengLong SHEN, JingNan GUO, QuanHao ZHANG, ZhengHua HUANG, Kai LIU, XiaoLei LI, Rui LIU, JingXiu WANG and Shui WANG

Articles you may be interested in

Concept of the Solar Ring Mission: Preliminary Design and Mission Profile
SCIENCE CHINA Technological Sciences

An overview of the mission and technical characteristics of Change'4 Lunar Probe
SCIENCE CHINA Technological Sciences **60**, 658 (2017);

Mission overview and key technologies of the first Mars probe of China
SCIENCE CHINA Technological Sciences **60**, 649 (2017);

Frontiers to be explored by the Parker Solar Probe mission
SCIENCE CHINA Technological Sciences **62**, 1481 (2019);

Enhance the performance of polymer solar cells via extension of the flanking end groups of fused ring acceptors
SCIENCE CHINA Chemistry **61**, 1320 (2018);

Concept of the solar ring mission: Overview

WANG YuMing[1,2]*, JI HaiSheng[3], WANG YaMin[4,5], XIA LiDong[6], SHEN ChengLong[1,2],
GUO JingNan[1,2], ZHANG QuanHao[1,2], HUANG ZhengHua[6], LIU Kai[1,2], LI XiaoLei[1,2],
LIU Rui[1,2], WANG JingXiu[7] & WANG Shui[1,2]

[1]*CAS Key Laboratory of Geospace Environment, School of Earth and Space Sciences, University of Science and Technology of China (USTC),
Hefei 230026, China;*
[2]*CAS Center for Excellence in Comparative Planetology, USTC, Hefei 230026, China;*
[3]*Purple Mountain Observatory, Chinese Academy of Sciences, Nanjing 210034, China;*
[4]*CAS Key Lab of Microsatellite, Innovation Academy for Microsatellites, Chinese Academy of Sciences, Shanghai 201203, China;*
[5]*Shanghai Engineering Center for Microsatellites, Shanghai 201203, China;*
[6]*Shandong Provincial Key Laboratory of Optical Astronomy and Solar-Terrestrial Environment, Institute of Space Sciences,
Shandong University, Weihai 264209, China;*
[7]*Univeristy of Chinese Academy of Sciences, Beijing 100049, China*

The concept of the Solar Ring mission was gradually formed from L5/L4 mission concept, and the proposal of its pre-phase study was funded by the National Natural Science Foundation of China in November 2018 and then by the Strategic Priority Program of Chinese Academy of Sciences in space sciences in May 2019. Solar Ring mission will be the first attempt to routinely monitor and study the Sun and inner heliosphere from a full 360-degree perspective in the ecliptic plane. The current preliminary design of the Solar Ring mission is to deploy six spacecraft, grouped in three pairs, on a sub-AU orbit around the Sun. The two spacecraft in each group are separated by about 30° and every two groups by about 120°. This configuration with necessary science payloads will allow us to establish three unprecedented capabilities: (1) determine the photospheric vector magnetic field with unambiguity, (2) provide 360-degree maps of the Sun and the inner heliosphere routinely, and (3) resolve the solar wind structures at multiple scales and multiple longitudes. With these capabilities, the Solar Ring mission aims to address the origin of solar cycle, the origin of solar eruptions, the origin of solar wind structures and the origin of severe space weather events. The successful accomplishment of the mission will advance our understanding of the star and the space environment that hold our life and enhance our capability of expanding the next new territory of human.

space mission concept, solar cycle, solar eruptions, solar wind, space weather

1 Introduction

As the development of technology, the boundary of human explorations was and is being constantly expanded, from continents, oceans, sky to space and even other planets. In near future, we believe, the deep space and other terrestrial planets, like Mars, will be the next new territory of human.

During the expansion of human activities into the deep space, we have to understand the Sun, interplanetary space and the space environments of the Earth and other planets.

Our Sun, the nearest star in the universe, primarily controls the electromagnetic radiation and particle radiation environments of the (inter)planetary spaces in either short term through various explosive activities or long term through solar cycles or even longer periodic variations. All these short

and long term activities can be treated as the manifestations and results of the changes of the magnetic field of the Sun. The huge amount of magnetic energy in the solar corona, accumulated due to the plasma flows in the lower solar atmosphere and/or even below photosphere, provides sufficient free energy for violent solar eruptions, e.g., flares and coronal mass ejections (CMEs). A typical solar eruption will release the energy of 10^{25} J in various forms along with the mass of 10^{12} kg and the magnetic flux of 10^{15} Wb [1], that will significantly disturb interplanetary space and may cause severe space weather events in the time scale from minutes to days.

Solar steady outflows and eruptions, making up the solar wind, travel through interplanetary space with a speed of more than hundreds of kilometers per second, and impact our planets. The *in-situ* observations of the solar wind in the past four decades have shown that the changes in magnetic field strength, plasma density, temperature and bulk velocity may exceed two orders of magnitude, and the flux of energetic particles can be enhanced by four or even larger orders during an event. Such large variations reflect the various levels of the energy and mass released from the Sun, and could severely affect the satellites and astronauts in the space. Thus, space weather forecasting has become an extremely important topic with significant application values for high-tech systems, especially for the human activities in the deep space.

The global and local dynamo processes make the solar activity gradually vary with multiple periods, among which the most famous one is the quasi-11-year solar cycle. About every 11 years, solar activity level increases from minimum to maximum and returns back to minimum accompanied with the reversal of magnetic field polarities between the south and north poles. Aforementioned solar eruptions are nearly ten times more frequent during solar maxima than during solar minima [2]. Solar interior structure and processes are one of the keys to understand these periods [3]. Besides, solar minima seemingly affect the space environment and the Earth's system, including the human society and civilization, more lasting and profound [4, 5] than solar maxima. In the last solar cycle, we experienced a deep solar minimum, which is the deepest in the past half of a century [6–8]. Will we experience another even deeper solar minimum and is this the start of a new little ice age [7, 9]? These questions have become the significant science issues of solar physics, space physics, and earth sciences.

These current knowledge of our Sun and (inter)planetary space are particularly owing to continuous space science missions in the past decades. From the view of Earth, we have the SOlar and Heliospheric Observatory (SOHO) [10], the Transition Region And Coronal Explorer (TRACE) [11], Yohkoh [12], the Solar Dynamic Observatory (SDO) [13], Hinode

[14], etc. Since the successful launch of the Solar TErrestrial RElations Observatory (STEREO) in 2006 [15], human for the first time watched the Sun and heliosphere simultaneously from two perspectives. In 2020, human will be able to obtain unprecedented images of the Sun off the ecliptic plane with Solar Orbiter (SolO) [16]. Except these imaging-enabled missions, we also have many space missions to sample local solar wind plasma, energetic particles and magnetic field, like the spacecraft Wind [17], the Advanced Composition Explorer (ACE) [18], the Deep Space Climate ObserVatoRy (DSCOVR) [19] at L1 point of the Sun-Earth system, the Helios [20] in the inner heliosphere, and the Ulysses [21] on a large elliptical polar orbit at about 5 AU. The recently launched Parker Solar Probe (PSP) will eventually fly to a distance of 8.5 solar radii from the Sun to sample the solar corona [22]. Besides, planetary science missions, e.g., the MErcury Surface, Space ENvironment, GEochemistry, and Ranging (MESSENGER) [23], the Venus Express [24], the Mars Express [25], and the Mars Atmosphere and Volatile Evolution (MAVEN) [26], provide additional information of the space environment near the planets. More than 20-year data from these great missions kept advancing our understanding on our Sun and (inter)planetary space.

However, we have not yet achieved the real-time observations of the full solar disk in 360°, which are essential to understand the whole evolution process of a sunspot, an active region (AR) and a coronal hole (CH) from their birth to death, to infer the solar internal structure, and to make long-term space weather forecasting possible. We have not yet achieved the unambiguous observations of the photospheric vector magnetic fields, which are the basis to understand all kinds of explosive phenomena on the Sun, and to realize how the local and global dynamos work. We have not yet achieved the routine observations combining the *in-situ* measurements and the remote panorama images of the solar wind and transients fully covering the inner heliosphere, which is the only way to understand the evolution of the solar outflows and eruptive structures, and to evaluate and forecast their space weather effects on our planets. Now we propose a new space scientific mission, Solar Ring, to accomplish the above capabilities.

2 Scientific rationale and mission objectives

The preliminary concept of the Solar Ring mission is to deploy 6 spacecraft circling around the Sun at a sub-AU distance in the ecliptic plane as illustrated in Figure 1(a). The idea was first from the L5/L4 mission concept, in which one spacecraft is suggested to operate at L5 point, the upstream of the Earth, to monitor the space weather in advance, and
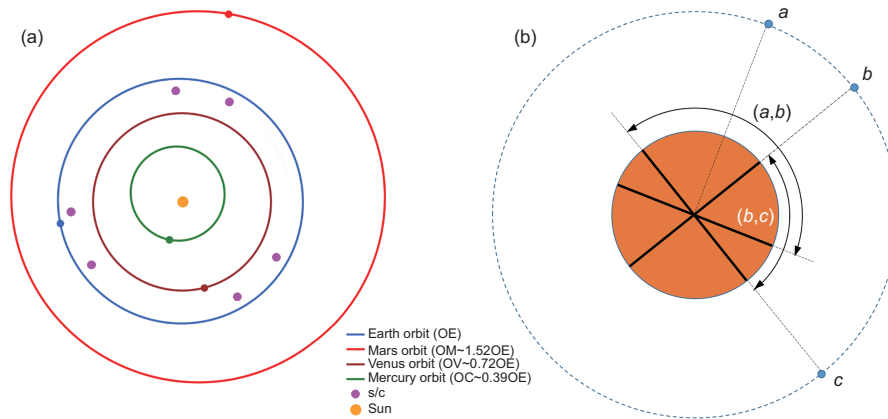
Figure 1   (a) Schematic diagram of the Solar Ring mission. The six pink dots roughly denote the positions of the six spacecraft, which run on a sub-AU orbit. (b) A sketch map illustrates the stereoscopic angles of the spacecraft and their coverage in the longitude.

one at L4 point, the downstream of the Earth, to get the effect of the space weather. The application value of such a mission is obvious and important. To enrich and enhance its science merits, we started to think about an upgraded one since the summer of 2017, and then gradually form the idea presented here, of which the scientific goals of L5/L4 mission are included and extended. Now the concept study has been funded by National Natural Science Foundation of China in the end of 2018 and by the Strategic Priority Program of Chinese Academy of Sciences in space sciences in early 2019.

The preliminarily designed orbit of Solar Ring, which is an elliptical orbit inside the Earth orbit (see Sect. 4 and the companion paper [27] for details), is a compromise between the scientific goals and the cost of the launch and transfer of the spacecraft. The spacecraft can self-drift to the desired position after being inserted into the orbit just like STEREO, that requires less fuel and can carry more scientific payloads. The six spacecraft are grouped in three pairs. In each pair, the two spacecraft are separated by about 30°, and between the pairs, the separation angle is about 120° (or about 90° between the two closest spacecraft). This deployment not only achieves the entire 360° view of the Sun, but also provides different stereoscopic views with the angle of about 30°, 90°, 120° and 150°. By using this configuration, Solar Ring mission will perform high resolution imaging of from photosphere to inner heliosphere and quasi-heliosynchronous *in-situ* sampling of particles and fields. The mission will address the following four major scientific themes:

- origin of solar cycle;

- origin of solar eruptions;

- origin of solar wind structures;

- origin of severe space weather events;

through the three unprecedented capabilities listed below.

2.1   Measure photospheric vector magnetic fields with unambiguity

Photospheric magnetic field is so far the only vector magnetic field in the space that can be remotely measured by human. Hence, it is so far the only key to understanding our magnetized star. The basic principle is that the spectral lines will split and get polarized in the presence of a magnetic field due to Zeeman effect. Though the Sun's magnetic field has been measured for more than 110 years, we still has not got accurate measurements of the photospheric vector magnetic fields without unambiguity. The main reason is that the direction of the transversal component has so called 180° ambiguity [28]. Besides, the transversal component of the measured photospheric magnetic field carries an uncertainty about one order higher in magnitude than the longitudinal (or line-of-sight) component.

The helioseismic and magnetic imager (HMI) [29] on board SDO measures the photospheric vector magnetic fields on the full solar disk. For example, Figure 2 shows the vector magnetogram of AR 12192 [30] and the scatter plots of the magnetic field strength in the AR and outside the AR, respectively. It is clear that the magnetic field inside the AR is highly structured but that outside the AR is random, indicating the noise. The horizontal lines in the bottom panels mark the 90-percentile of the magnetic field strength, which could be treated as the uncertainty of the measurements. For the longitudinal component (Figure 2(d)), the uncertainty is less than 40 G, whereas that of the transversal component is about 100 G. Since the photospheric magnetic fields in quite Sun regions and CHs are typically of the order of ten Gauss, the measured transversal component is only reliable and applicable in ARs, where the magnetic field is strong enough. It should be aware that the observed magnetic field strength mentioned here is actually the magnetic flux density, an
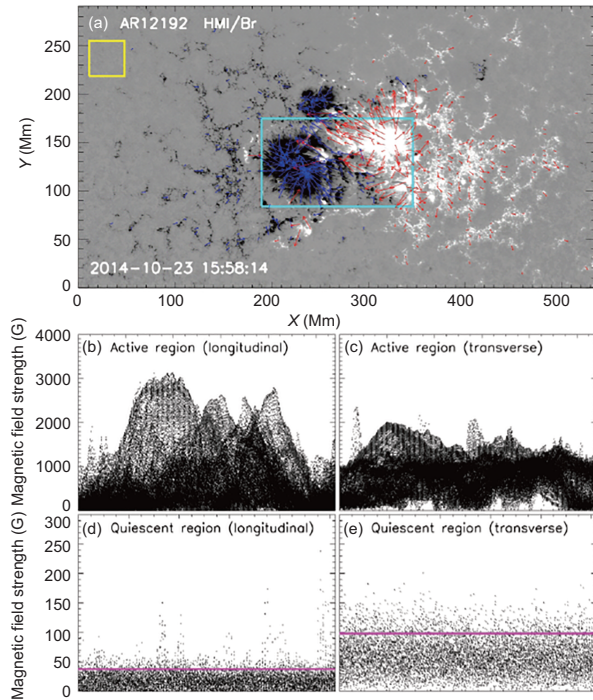
Figure 2   (a) The HMI vector magnetogram of the active region NOAA 12192. The gray color scales the longitudinal component of the magnetic field, and the red/blue arrows denote the transversal component. (b), (c) Scatter plots of the longitudinal and transversal components of the magnetic field in the central region marked by the cyan box in (a). (d), (e) The same scatter plots, but in the region near the edge marked by the yellow box in (a). The horizontal axes in (b)–(e) mark the serial numbers of the data points in the data set, having no physical meaning. The magnetic field within the active region is highly structured, but that in the quiescent region is more close to noise. The horizontal pink lines denote the 90-percentile of the magnetic field strength, suggesting the noise level.

average of the magnetic fields over a certain area depending on the spatial resolution. Using high-resolution observations, magnetic fields as high as hundreds of Gauss are often found in quiet Sun regions [31].

Above the photosphere, there are the chromosphere, transition region, corona and interplanetary space, where more key processes of the solar eruptions, coronal heating and solar wind acceleration happen. However, due to the low density, high temperature and highly dynamic atmosphere above the photosphere, the three dimensional (3D) magnetic field has never been precisely measured. Most of the information of the coronal magnetic fields come from the extrapolation of the photospheric magnetic fields [32]. Non-linear force-free field (NLFFF) extrapolation is a widely used approach to reveal the evolution of the coronal magnetic energy before and after an eruption. All the force-free field extrapolations are model dependent. As a most widely used NLFFF model developed by Wiegelmann [33], for instance, it has been successfully applied to study many solar eruptive events. A re-

cent application of this model is to identify and study the solar magnetic flux ropes during an eruption, but an interesting thing is that none of the identified magnetic flux ropes stays above 10 Mm from the solar surface, inconsistent with the frequently-found high lying prominences/filaments. This is due to the treatment of energy minimization when processing photospheric vector magnetograms, which is basically the limitation of the presence of the 180° ambiguity in the transversal component. Thus, such inaccurate measurements of photospheric vector magnetic fields largely limit our understanding of the solar activities.

For remote sensing, the only way to remove the 180° ambiguity and increase the measurement accuracy is the multiple-perspective observation. Three spacecraft forming a solid angle of a certain value (not too small and not too large) to observe circular polarization will be the cleanest way to accurately map magnetic fields of the photosphere. However, since flying away from ecliptic plane is technically difficult and very expensive, two spacecraft observing both circular and linear polarization will be the feasible plan for us to remove the 180° ambiguity (the detailed analysis is being prepared in the follow-up paper[1]). Though STEREO spacecraft have been able to view the Sun from two perspectives off the Sun-Earth line since 2006, unfortunately they did not carry a magnetic imager. Our mission will solve this issue by providing vector magnetic observations from multiple perspectives as mentioned above. In principle, if there are vector magnetic measurements from two viewing angles as illustrated in Figure 3, the magnetic field vector can be inversed by using the formulae

$$\begin{cases} \mathbb{M}^a \mathbf{B} = B_{\mathrm{L}}^a \hat{r}^a \pm \mathbf{B}_{\mathrm{T}}^a, \\ \mathbb{M}^b \mathbf{B} = B_{\mathrm{L}}^b \hat{r}^b \pm \mathbf{B}_{\mathrm{T}}^b, \end{cases} \qquad (1)$$

where $\mathbb{M}$ is the transform matrix, B_{L} and $\mathbf{B}_{\mathrm{T}}$ are the longitudinal and transversal components of the measured magnetic field, respectively, $\hat{r}$ is the longitudinal direction, and the
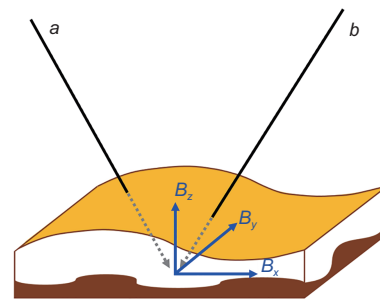

Figure 3   A cartoon of the local photospheric region, illustrating some issues affecting the accuracy of the inversion of magnetic field from dual perspectives. The black arrows *a* and *b* indicate the observational paths. The photosphere is a non-uniform layer with different optical depths.

superscripts *a* and *b* indicate the two different perspectives. The 180° ambiguity can be solved. Moreover, a part of the transversal component of the magnetic field from one perspective is a part of the longitudinal component from the other. The uncertainty of the transversal component therefore can be reduced to some extent. Thus, multiple-perspective measurements will provide us unprecedented insight into the evolution of the magnetic field from photosphere to corona.

But some issues exist and may affect the accuracy of the inversion of the magnetic field[1] As indicated in Figure 3, for example, the observational paths, heights of the emission source and the optical depths from different perspectives are different though they aim to the same region. Thus, the measured vector magnetic field of the same region could be theoretically different. The significance of these effects depends on the separation angle of the two spacecraft. Obviously, the less the separation angle is, the weaker are the effects. But if the separation angle is too small, the dual perspectives will reduce to a single perspective considering the uncertainty in the measurements. Thus, the question is what the optimal separation angle is between two spacecraft. In the current design, the separation angle is 30° in each group and 90° between groups as illustrated in Figure 1(b). Intuitively, the 30° separation is better than the 90° separation: not only the inversion of the vector magnetic field could be more accurate, but also the overlapped solar surface is wider.

It is worth to note that SolO by European Space Agency (ESA) was successfully launched on 10 February 2020. It together with SDO at Earth will achieve the dual-perspective magnetic field observation for the first time. Since the orbit of SolO is not in the ecliptic plane but has the inclination of about 25° and perihelion of about 0.28 AU, the separation angle between SolO and SDO varies greatly. This causes that the accurate vector magnetic fields can not be routinely obtained, which will be regret for the study of the global evolution or that of a particular region not within the time window of the dual-perspective observations. But they will provide us opportunities to study the influence of the separation angle on the inversion of the vector magnetic fields based on measured data. Besides, SolO gives the perspective out of the ecliptic plane, which will be valuable addition to our Solar Ring mission. Combining the measurements of the magnetic fields from three perspectives not lying on one plane, we theoretically can obtain vector magnetic fields only based on the observations of the longitudinal components, which are more accurate than transversal components, as follows:

$$
\begin{cases}
\mathbf{M}_L^a \mathbf{B} = B_L^a, \\
\mathbf{M}_L^b \mathbf{B} = B_L^b, \\
\mathbf{M}_L^c \mathbf{B} = B_L^c,
\end{cases}
\tag{2}
$$

where $\mathbf{M}_L$ is the longitudinal component of the transform matrix $\mathbb{M}$. The inversion of the vector magnetic field should be even more accurate.

2.2 Provide 360-degree maps of the Sun and the inner heliosphere

Multiple-perspective observations of global oscillations, which can be obtained when measuring the photospheric vector magnetic fields, are especially important to helioseismology for studying the Sun's deeper interior and higher latitude. Currently, all our knowledge on the Sun's interior structure and dynamics either relies on theoretical modeling [34] or one-side observations of the Sun. The one-side helioseismic observations, which routinely started in mid-1990s [35, 36], allow us to infer the Sun's internal differential rotation up to the bottom of the convection zone [37, 38], and also allow us to start understanding the meridional circulation inside the Sun [39]. However, what the differential rotation is like beneath the convection zone and in higher latitude above 60° is largely unknown. More importantly, despite the crucial role of meridional circulation in transporting magnetic flux inside the Sun, our current understanding of the meridional-circulation structure is by far unsatisfactory. All these are limited by our limited capability of only simultaneously observing limited areas of the Sun, with acceptable spatial resolutions only within about 60° from the Sun's apparent disk center. Solar Ring mission will allow us to simultaneously observe the Sun from multiple perspectives with various angles including some greater than 120°, providing crucial data for the deeper interior as well as higher latitude. A well-determined solar interior rotational profile and meridional-circulation profile will allow us to better understand the Sun's dynamo and its generation of magnetic cycles [40].

On the other hand, most notable solar activities are global behaviors. Sympathetic eruptions, for example, are often observed [41–43], which occur in different ARs but almost simultaneously, suggesting connections and interactions between different ARs. Such connections and interactions could be global and not just between neighboring regions. As a case studied in the paper [44], the major events during 2011 August 1–2, spreading over more than a quarter of the solar surface in longitude, were connected via large-scale separators, separatrices and quasi-separatrix layers (see Figure 4). Even in single eruptions, inter-region connections could be often identified [45]. Statistical study also showed that one third of all ARs present transequatorial loops [46]. These facts require a 360°-view of the Sun to completely and correctly understand such large-scale eruptive phenomena, including their causes and effects.

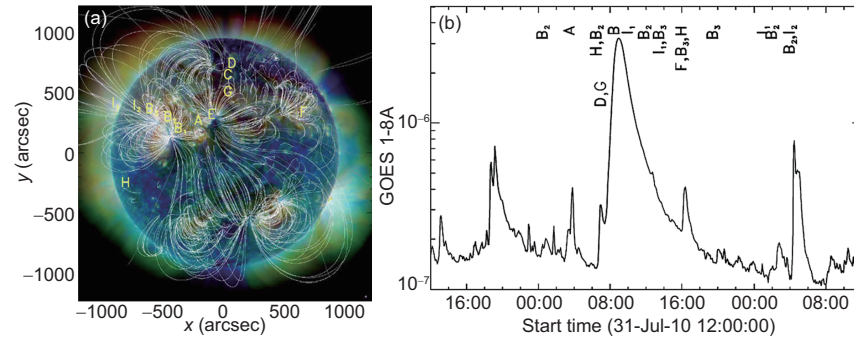Not only such widely-spread sympathetic activities, but

Figure 4   (a) Three-color composite EUV image combined from SDO/AIA 211 Å, 193 Å, and 171 Å channels on 1 August 2010. Coronal magnetic field lines extrapolated using a potential field source surface (PFSS) model are superimposed, showing the magnetic connections among different regions. Letters denote the locations of the eruptive events during 1–2 August 2010. (b) GOES 1–8 Å light curve with the same denoted letters. Adapted from ref. [44].

also long-term (weeks to months) evolving solar structures and features, e.g., filaments, sunspots, ARs and CHs, require the 360° view. For instance, the long-lived CH investigated in the paper [47] evolved for 10 solar rotations from its growing phase to its maximum and decaying phases. All these long-term evolving structures are controlled by the evolution of magnetic field and essentially by the solar dynamo. So far the global photospheric magnetic field map, so called synoptic chart [48], is a kind of summary map of the sampled photospheric magnetic field over a solar rotation. Global extrapolation of coronal magnetic field is based on such a synoptic chart. Without a realtime map, some details especially those on the backside of the solar disk will be missed and the extrapolation will be inaccurate.

From the 360° maps of the Sun from multiple perspectives, we may also derive the 3D information of various structures and features in the solar atmosphere, such as the coronal loops [49], solar jets [50], bright points [51], etc. As illustrated in Figure 1(b), each group of the spacecraft may cover nearly 150° in longitude, and three spacecraft may cover 180°. Of course, the inversion of the 3D magnetic field and coronal structures will become unreliable close to the edge of the common field of view (FOV). Thus, 150° and 180° are the upper limits in theory. But these gaps can be filled by other three spacecraft in the Solar Ring mission. Then we can do what was never done before, e.g., to link different eruptive activities scattered over the solar surface into one story, to trace the whole life of an AR or a CH from its birth to death at multiple wavelengths, to trace how magnetic fluxes transport from low latitude to high latitude and vise versa, and to forecast potential space weather events in much more advance.

Between the Sun and planets including the Earth, there is a big gap—interplanetary space or the heliosphere, where the solar wind and various eruptive transients travel through all the time. From the perspective of Earth, Earth-directing CMEs that most likely to cause severe space weather events might be missed due to projection effect [52]. A statisti-

cal study suggested that about one third of frontside CMEs were missed by the coronagraph LASCO on board SOHO [53]. STEREO watching the corona and inner heliosphere from two perspectives greatly reduce the projection effect, and make most Earth-directing CMEs visible. Moreover, the 3D morphology and kinematics of various solar wind transients, including CMEs, blobs and shocks, are able to be obtained from the dual-perspective imaging data [54–57]. The recent method based on Correlation-Aided Reconstruction (CORAR) technique [58, 59] allows us to automatically recognize and locate inhomogeneous structures in solar wind without any preset assumptions on the morphology. Figure 5 shows a CME (and three blob-like transients, not shown in the frame) propagating in the common FOV of HI-1 cameras
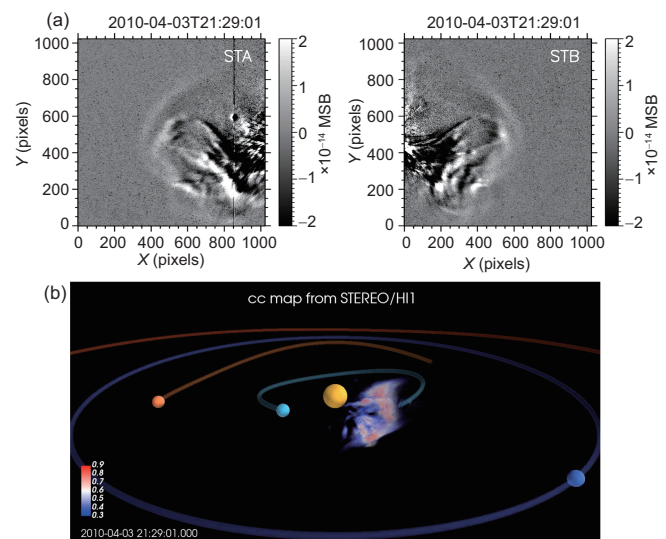

Figure 5   (a) The running-difference images of the heliosphere taken by HI-1 cameras on board the STEREO A and B spacecraft at 21:29 UT on 3 April 2010. A CME was captured. (b) The correlation coefficient (cc) map of the heliosphere at the same time, inferred from the HI-1 images through CORAR method. The CME is reconstructed in the high cc region. The yellow, cyan, orange and blue balls denote the Sun, Mercury, Venus and Earth. Adapted from the paper [58].

of STEREO on 2010 April 3 and the reconstruction by the CORAR technique, which is quite consistent with the observations and other models [58]. However, the common FOV of STEREO is limited to the region between the Sun and Earth. Some large-scale structures often exceed or even travel beyond the common FOV though they might also impact and affect the Earth's space environment [60]. Thus, to have a panoramic 3D view of the inner heliosphere, more spacecraft, like the deployment of Solar Ring, is necessary. A more detailed analysis of the optimal separation angle between the spacecraft for the the CORAR technique is given in the paper[2].

A panoramic view of the inner heliosphere is important to understand the dynamic evolution of solar wind transients in interplanetary space and consequent space weather effects. The outstanding questions include how the morphology and trajectory of solar wind transients change during the propagation [61–65], how the transients are accelerated or decelerated [66–69], how the transients exchange magnetic flux with ambient solar wind [70–72], how the transients interact with each other and cause the changes in velocity and direction [73–76], etc. All these are closely-related to and partially determine whether, when and how significantly severe space weather will occur.

2.3 Resolve solar wind structures at multiple scales and multiple longitudes

Solar wind structures including steady structures, e.g., heliospheric current sheets and corotating interaction regions (CIRs) forming between fast and slow solar wind, and aforementioned transients, e.g., blobs, CMEs, magnetic clouds and shocks, originate from the Sun and gradually propagate and expand into the heliosphere. The macroscopic scale of them is very large. CMEs and magnetic clouds are all thought to be magnetic flux ropes with their two legs still connected to the Sun even at the distance of 1 AU [77]; the angular width of them is typically 60° [2, 53], and the radius of the cross-section is about 0.1 AU on average at the heliocentric distance of 1 AU [78].

Such a large-scale structure may manifest different properties and behaviors at different parts. Magnetic flux rope, for example, is a fundamental plasma structure, and twist of magnetic field lines inside a interplanetary flux rope is a key parameter to characterize its property and stableness and to understand its origin and initiation from the Sun [72, 79] (Figure 6). However, it is not clear if the twist is uniformly distributed in flux ropes. It is a debate whether or not the field
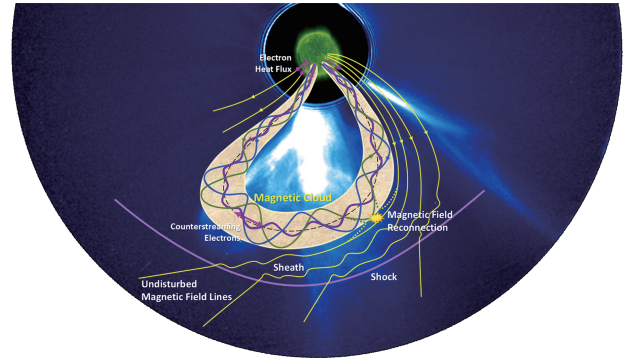

Figure 6   A cartoon showing the large-scale magnetic flux rope, or called magnetic cloud, in the heliosphere. The magnetic field lines are twisted in the magnetic cloud as indicated by the color-coded lines. The reconnection site implies the erosion process. A shock exists if the magnetic cloud propagates fast. Adapted from ref. [72].

lines are more twisted in the leg than in the apex of a flux rope [79–81]. Moreover, magnetic clouds are thought to be a coherent flux rope structure originating from the Sun, but it is difficult to identify the same magnetic cloud structure from different spacecraft if the spacecraft separate too widely [82]. Is it due to the loss of the coherency during the propagation in interplanetary space [83] or the strong modulation by ambient solar wind?

Interplanetary solar energetic particles (SEPs), with energies from a few keV up to relativistic GeV are generally accelerated during solar eruptions by either the magnetic reconnection processes and/or CME-driven shocks. SEPs generated by shocks are of particular interest since protons can reach energies larger than 10 MeV posing serious radiation threats to human exploration activities in space and causing technological and communication issues to satellites [84]. However, we have not yet obtained a complete understanding of these large SEP events since their properties, normally observed from one viewpoint of Earth, are a complex mixture of several important physical processes: acceleration, injection and transport. These processes are evolving in time and location-dependent and are determined by the macro-structures of the shock and the heliosphere as well as the micro-properties of the particle scattering and transport procedure. As a consequence, the distribution of the flux of the energetic particles at different heliospheric longitude and radial distance may be quite different [85], causing significantly different radiation environment at different planets. A recent work using multiple spacecraft showed that a complex CME structure led to a solar energetic particle event not only at Earth but also at Mars and STEREO A, across a heliospheric longitude span of 230° [86]. However, SEP energy spectra and temporal evolution are different at each of the three ob-

---

servers as shown in Figure 7 [86, 87]. It is an interesting and important issue how energetic particles transport from initial direction to such a wide longitude range.

Many macroscopic properties are linked with microscopic processes, but in lack of details. For example, the dramatic expansion of CMEs in interplanetary space may cause significant decrease of the internal temperature if no additional heat source exists. However, the *in-situ* measurements at 1 AU show that the temperature is not low enough, suggesting a heating process. With the aid of an observation constrained model, it was revealed for two CMEs that the polytropic index of the CME plasma is well below the adiabatic index 3/5, also suggesting the heating [88, 89]. What is the mechanism of the heating? Is it due to the wave-particle interaction or direct injection of thermal electrons? Erosion of magnetic clouds has been proven a common phenomenon in interplanetary space [71], suggesting a strong exchange of the magnetic flux between the magnetic cloud and ambient solar wind. Its macroscopic manifestation is that a magnetic cloud can be peeled off when it is propagating outward until merging into solar wind, while the microscopic manifestation is the appearance of signatures of magnetic reconnection, i.e., the exhausting region, at the boundary of the magnetic cloud [90, 91]. But without multiple spacecraft at different positions, it is hard to learn if the erosion process is a local phenomenon or a global phenomenon, and if there are many exhausting regions spreading on the outmost surface of the magnetic cloud. The same issue exists when studying the plasma motion inside magnetic clouds [78, 82], of which the cause is unclear.

Besides, the momentum transfer and energy conversion of solar wind transients with ambient solar wind and other transients are still puzzling in many events. The collision/interaction between two CMEs in inner heliosphere was never thought to be super-elastic before the 2008 November 2 event was analyzed based on imaging data [73] and numerical simulations [92]. However, due to the absence of the

in-situ measurements of the event, the details of the process and mechanism of how and why the total kinetic energy of the two CMEs was gained are still missing. Thus, *in-situ* measurements at different positions as well as global pictures are required to better understand all of the above issues. The former is used to obtain accurate plasma and magnetic field parameters, and the latter is to constrain global morphology of the large-scale structure, which may provide additional information about the dynamic and thermodynamic processes of the structure, e.g., the acceleration/deceleration process, pancaking or distortion process, erosion process, deflection process, interaction/collision process, etc.

There are events well observed by multiple spacecraft in both imaging data and *in-situ* measurements, but the number is small. The configuration of the Solar Ring mission will make such kinds of observations routine. As mentioned before, the angular width of CMEs are typically 60° [53], wider than the separation angle of the spacecraft in each group of the Solar Ring mission. Shocks and resulted particle events could span even wider, and therefore the spacecraft belonging to different groups with the separation angle of 90° or 120° could be ideal probes to measure them simultaneously. Other spacecraft then take pictures from side-view to provide global information of the events. With this capability, the understanding of the solar wind structures and the level of space weather forecasting will be greatly advanced.

3   Scientific instruments and requirements

To achieve the above capabilities in accurately measuring photospheric vector magnetic fields, providing 360° panoramic pictures of the Sun and the inner heliosphere, and resolving solar wind structures at multiple scales, and then further to tackle the science objectives, we need remote sensing data, including spectral observations for the solar magnetic fields, multi-band observations for the solar EUV emissions, white-light observations for the corona and inner he-
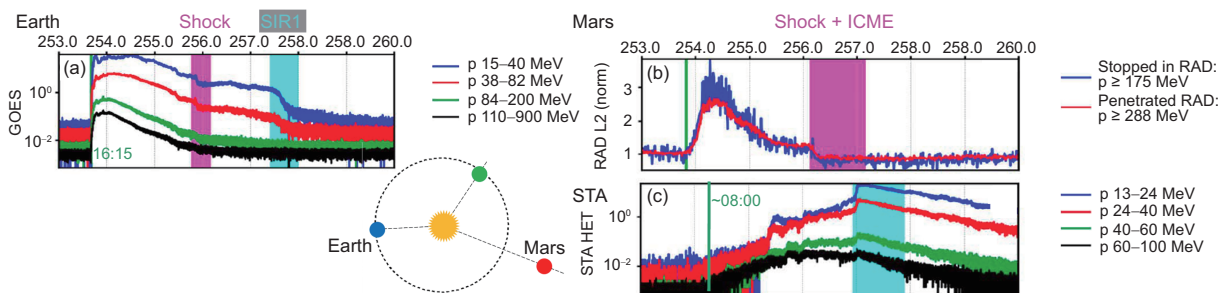

Figure 7   The fluxes of energetic particles recorded by (a) GOES at Earth, (b) Radiation Assessment Detector (RAD [87]) at Mars and (c) STEREO A during 10–16 September 2017. The pink region indicates the shock (and CME) arrival, and the cyan region the stream interaction region. The positions of the Earth, Mars and STEREO A on 10 September 2017 are plotted too. A complex solar eruption caused the enhancement of the fluxes in a wide range. Adapted from ref. [86].

liosphere, and the radio emissions, and also *in-situ* measurements of the solar wind magnetic field, solar wind plasma and energetic particles. The relationship between the science objectives and these measurements is summarized in Table 1.

These measurements are suggested to be accomplished by the following science payloads onboard each of the spacecraft of the Solar Ring mission (refer to Table 2). First of all, the spectral imager for magnetic field and helioseismology (SIMS) provides the measurements of the vector magnetic field and Doppler shift information on the photosphere. It is

Table 1 Science objectives and required measurements

Science objectives	Scientific questions	Strategy	Solar magnetic field & global Doppler velocity	Solar EUV images	White-light images	Radio emissions	Solar wind magnetic field	Solar wind plasma	Energetic particles
Origin of solar cycle	How does the global magnetic flux emerge, transport and dissipate?	Trace the global magnetic fluxes at multiple scales.	√						
	What is the solar internal structure?	Analyze the global oscillation modes.	√						
Origin of solar eruptions	How is the energy accumulated and released, and how is an eruption triggered?	Trace the evolution of source region and combine measured magnetic field, radio emissions and energetic particles to estimate some key parameters, e.g., the magnetic energy and helicity, and key processes.	√	√		√			√
	How are the coronal structures reconstructed, and what kind of structures are formed and ejected into heliosphere?	Extrapolate coronal field and compare with observed coronal plasma structures in EUV, compare erupted signatures in EUV and white-light images.	√	√	√				
Origin of solar wind structures	Where does an solar wind structure come from? What's its topology and magnetic connection with the Sun? How does a solar wind structure evolve in the heliosphere in terms of its propagation direction, velocity, topology, etc?	Use white-light images from multiple perspectives to recognize and reconstruct solar wind structures in interplanetary space and trace their evolution. Associate the imaging data of solar wind structures to *in-situ* data at 1 AU to confirm their properties, and trace back to the Sun to obtain the properties of their sources.	√	√	√	√	√	√	√
Origin of severe space weather events	What are the primary factors causing major geomagnetic storms and/or solar energetic particle events?	Investigate *in-situ* data, including magnetic field, solar wind plasma and energetic particles, at different longitudes to assess the effects of various factors on the space weather.			√		√	√	√
	What are the properties of the source regions of the drivers of severe space weather? How can we make an accurate forecast of the space weather effects of solar eruptions?	Use imaging data of the heliosphere and the Sun to identify the source regions of the space-weather-effecting solar wind structures and to study the relationship between the solar eruptions and space weather events.	√	√	√	√	√	√	√

Table 2 Main tasks and preliminary technical specifications of payloads (to be continued)

Payloads	Main tasks	Preliminary technical specifications
Spectral imager for magnetic field and helioseismology (SIMS)	Measure photospheric vector magnetic field to learn the global transportation of magnetic flux; measure global Doppler velocity to learn the global oscillations.	Mass: ⩽ 30 kg Power consumption: ⩽ 40 W Data rate: ⩽ 30 Mbps (@peak time) Field of view: 32′ × 32′ (@1 AU) Effective pixels: no less than 4096 × 4096 Spectral resolution: better than 0.04 Å Temporal resolution of longitudinal component: 1 min, 1 h Temporal resolution of transversal component: 2 min, 1 h
Multi-band imager for EUV emissions (MIE)	Obtain the global EUV images of solar disk at three wavelength bands, corresponding to relatively cool, warm and hot temperatures, respectively, to learn the morphology, topology, connectivity and emission measure of various plasma structures.	Mass: ⩽ 30 kg Power consumption: ⩽ 60 W Data rate: ⩽ 21 Mbps (@peak time) Field of view: 42′ × 42′ (@1 AU) Effective pixels: no less than 4096 × 4096 Wavelength bands: 304 Å, 171 Å, 131 Å Temporal resolution: 10 s, 1 min, 1 h
Wide-angle coronagraph (WAC)	Obtain white-light images of the solar wind structures traveling through the outer corona and inner heliosphere to learn their kinematic properties; get total brightness and the variations to learn the density distribution in 3D.	Mass: ⩽ 25 kg Power consumption: ⩽ 40 W Data rate: < 1 Mbps (@peak time) Field of view: ±12° Occulting disk: ±2° Effective pixels: no less than 4096 × 4096 Temporal resolution: 1 min, 1 h
Radio investigator (WAVES)	Measure the electric field intensity induced by the radio emissions from the Sun to recognize the radio bursts and get the location of the driving source and its kinematic properties.	Mass: ⩽ 15 kg Power consumption: ⩽ 16 W Data rate: 0.5 kbps Frequency range: 5 kHz–30 MHz Frequency channels: no less than 160 Temporal resolution: better than 30 s GP mode: 0.2 s for each channel/antenna configuration
Flux-gate magnetometer (FGM)	Measure the *in-situ* magnetic field at 1 AU to learn the variations during solar wind structures and the distribution in longitude.	Mass: ⩽ 2 kg Power consumption: ⩽ 3 W Data rate: ⩽ 8 kbps Maximum measuring range: ±65000 nT Dynamic measurement range: 2000 nT Resolution: better than 0.01 nT Noise level: better than 0.01 nT/$\sqrt{\text{Hz}}$ Zero drift: better than 0.01 nT/°C Sampling rate: 0.1 Hz, 128 Hz
Solar wind plasma analyzer (SPA)	Measure the *in-situ* solar wind plasma at 1 AU; obtain the velocity, density, temperature and composition of the solar wind to learn the variations during solar wind structures and the distribution in longitude.	Mass: ⩽ 7 kg Power consumption: ⩽ 20 W Data rate: ⩽ 50 kbps Field of view: 180° (azimuthal angle) × ±45° (polar angle) Angular resolution: better than 12° (azimuthal) × 15° (polar) Temporal resolution: 4–64 s (adjustable) Ions • Energy range: 0.1–25 keV • Energy resolution: better than 12% • Energy channels: no less than 64 • Mass range: 0–60 amu • Mass resolution: better than 18% Electrons • Energy range: 0.05–10 keV • Energy resolution: better than 12% • Energy channels: no less than 64
High-energy particle detector (HiPD)	Measure energetic particles in multiple energies to obtain the intensity and spectrum of a solar energetic particle event and to learn its driver and the distribution in longitude.	Mass: ⩽ 1 kg Power consumption: ⩽ 1 W Data rate: ⩽ 1 kbps Field of view: 55° cone Mass range: 0–60 amu, electrons Energy range of • Electrons: 0.5–20 MeV • Protons: 10–100 MeV • Heavy ions: 20–200 MeV/nuc
Total	Mass: ⩽ 110 kg, power: ⩽ 180 W, data rate: ⩽ 52.06 Mbps	

one of the most important payloads regarding the four science objectives: the origin of the solar cycle, the origin of the solar eruptions, the origin of the solar wind structures and the origin of the severe space weather events. SDO/HMI can provide the 4096×4096 vector magnetogram of the full photosphere every 45 s in the longitudinal component and every 135 s in the transversal component. Such cadences and spatial resolution are able to reveal the magnetic evolution and therefore the accumulation process of magnetic energy before an eruption, and are sufficient for the study of the solar cycle. Considering the orbit of the designed Solar Ring spacecraft, which will be discussed in the next section, being much farther than that of SDO and limiting the data transmission rate, the cadence of SIMS is set to close to that of HMI when the spacecraft close to the Earth and 1 h or longer at far side.

The multi-band imager for EUV emissions (MIE) provides the condition and evolution of the plasma structures in the solar atmosphere, where are necessary to see the effect of the evolution of photospheric magnetic field. The spatial resolution is the same as SIMS. With images from multiple perspectives, the 3D topology of plasma structures can be revealed, of which the process is similar to those done by using STEREO and/or SDO data [49]. These data provided by MIE are key to understand the eruptive phenomena in the solar corona and also to locate the solar source of the solar wind structures traveling in the outer corona and inner heliosphere. Three wavelength bands are suggested: (1) 304 Å, a relative cool line for the chromosphere and transition region, particularly suitable for filaments/prominences; (2) 171 Å, a relatively warm line for the corona, good for coronal loops, post-flare arcades, etc.; and (3) 131 Å, a relatively hot line for flaring regions with a warm component less than 1 MK, best for hot channels and other heated structures.

The wide-angle coronagraph (WAC) provides the situation of the outer corona through inner heliosphere, bridging the Sun and inner planets, including Mercury, Venus, Earth and probably Mars. The white-light images taken by WAC are necessary to identify the consequence of the solar eruptions in interplanetary space and the source of space weather events. The data from multiple spacecraft can be further used to retrieve the 3D information of solar wind structures. The brightness of solar wind decreases quickly with increasing distance away from the Sun, causing strong contrast between near-Sun side and far-side. The signal-to-noise ratio decreases too with increasing distance, and particularly beyond elongation angle of $20°$, it becomes too low to perform a reliable reconstruction [58]. To reach a compromise among the wide FOV, the acceptable contrast and the sufficient signal-to-noise, WAC is suggested to have an outer FOV of about $\pm12°$ in elongation angle and an inner FOV of

about $\pm2°$, covering the region from about 7.5 to $45R_S$ in the plane-of-the-sky from 1 AU (or about 5.6 to $34R_S$ from 0.75 AU). This region is best for the study of solar wind transients in 3D as most of them have been well developed and entered the cruise phase. Due to the large scale of the structures, the cadence of the images could be tens of minutes depending on the signal-to-noise and the data transmission rate.

The radio investigator (WAVES) is deployed to monitor the high-energy phenomena occurring on the Sun and in interplanetary space. Solar flares will cause Type III and Type IV radio bursts, and fast-forward shocks driven by CMEs will cause Type IIs. These bursts leave distinguished drift patterns in the radio dynamic spectrum from GHz to below MHz, providing additional diagnose of solar eruptions. The WAVES is preliminarily designed to receive the radio signal from 30 MHz to 5 kHz, slightly wider than Wind/WAVES and STEREO/WAVES, covering the heliocentric distance from about $1.5R_S$ to 1 AU in terms of the electron plasma frequency. When multiple spacecraft receive the same burst, its radio source region could be located by using a triangulation method [93–96]. The method in the paper [96] showed that the 1-min temporal resolution of the radio intensity spectrum can be used to locate the source about $25R_S$ away from the Sun if the spacecraft are separated by more than $60°$. The wider the spacecraft are separated, the lower temporal resolution is sufficient. Thus, we suggest the temporal resolution of final radio dynamic spectrum should be better than 30 s to locate the source region closer to the Sun. Besides, more information of the radio emission, e.g., the polarization properties, need the instantaneous goniopolarimetric (GP) capability (also know as direction-finding capability) of the radio receivers [97]. It requires rapid switch between the channel/antenna configurations about every 0.2 s, which should also be equipped. This capability will also increase the accuracy in locating the source region of a radio burst, benefitting the space weather forecasting.

The rest of the payloads are for *in-situ* measurements to provide a more complete picture of the conditions of the inner heliosphere. As one of the fundamental parameters characterizing the solar wind conditions, the interplanetary magnetic field is typically 10 nT on average, and sometimes can reach up to hundreds of nT. For solar wind transients which are large-scale structures, the sampling rate of magnetic field does not need to be too high. But for microscopic phenomena and process, e.g., the shock front, reconnection exhausting region and turbulence, a high sampling rate of magnetic field is required. The previous studies have shown that the wave energy carried by the solar wind cascades from large scale to small scale in inertial range of the wavelength, and reaches the dissipation range, which is typically beyond 1 Hz

[98]. Thus, the flux-gate magnetometer (FGM) is suggested to be deployed to sample the magnetic field with the rate of 0.1 or 128 Hz (depending on the data transmission rate) and the resolution of 0.01 nT.

The solar wind plasma analyzer (SPA) measures the *in-situ* plasma in the energy range from 0.1 to 25 keV for ions and 0.05 to 10 keV for electrons. This energy range covers the main flux of the solar wind plasma, providing other basic parameters, e.g., the bulk velocity, density and temperature, of the solar wind conditions. Solar wind outflow has two components. One is the beam almost along the Sun-observer line, and the other is the halo mostly coming from the Sun-ward half sky due to the scattering and diffusion. Thus, the SPA is designed to receive particles with the FOV of 180° (azimuthal angle) × ± 45° (polar angle) [99]. Further, to diagnose the source of solar wind, e.g., CHs or ARs, steady flow or transients, the capability of measuring the mass and charge state is required to distinguish helium, carbon, oxygen through iron ions. The temporal resolution ranges from seconds to minutes.

The high-energy particle detector (HiPD) is dedicated to the study of the particle acceleration and transportation and the solar energetic particle events, related to three of the four science objectives as indicated in Table 1. The HiPD is designed similar to the high energy telescope (HET) on board the SolO mission, consisting of four 300 μm thick silicon solid state detectors (SSDs) and one high-density scintillation crystal. It measures electrons, protons, and heavy ions. Electrons are covered across the energy range from 500 keV up to about 20 MeV; protons are measured between 10 and 100 MeV and heavy ions from about 20 to 200 MeV/nuc. HiPD also needs to separate ^{3}He and ^{4}He isotopes which is important in differentiating the acceleration process of flare or shock related SEPs. During solar quiet times, the study of these particles as present in galactic cosmic rays (GCRs) can also help to understand the transport of GCRs inside the heliosphere. The HiPD unit will be located on each of the six Solar Ring spacecraft with the central FOV pointing sunward/anti-sunward direction of the Parker Spiral and a view cone of about 55°. The sunward direction will allow the detection of the beam SEPs which are the earliest arriving ones during an event especially when the observer is well connected to the acceleration. The anti-sunward direction will allow the detection of back scattered particles which are excellent tracers of the magnetic topology and large scale connectivity of the interplanetary magnetic field [100].

In total, the mass of the suggested payloads of each spacecraft is 110 kg, the power requirement is 180 W, and the data rate at peak time is 52.06 Mbps. The data rate might be too high to achieve based on the current technology. Thus, how

to reduce and compress the data or to develop a new technique to communicate with the spacecraft is a big challenge, and will be studied in the future.

4   Mission profile and design

There are several factors defining the basic outline of the Solar Ring mission. (1) The number and separation angles of the spacecraft. As mentioned before, the number is six and the separation angles of them are about 30° in each group and 120° between groups as shown in Figure 1. The orbit is within 1 AU, and could be a circular orbit or elliptical orbit. A circular orbit may provide a more consistent FOV among the spacecraft than an elliptical orbit, and be more convenient for and more accurate in the analysis of the data from multiple perspectives. However, to deliver spacecraft into a circular orbit consumes more fuel than into an elliptical orbit. (2) The time to deploy all the spacecraft. The science objectives require all the spacecraft working together. For some objectives, at least two spacecraft are required. Considering the lifetime of each spacecraft, it is better deploy all the spacecraft within a short time. The scheme of one rocket two spacecraft or even four spacecraft can deploy the mission fast, but needs larger rocket thrust that reduces the capability of carrying payload. (3) The mass of the spacecraft. The dry mass of a spacecraft without payloads is at least 350 kg. Plus the suggested payloads, the total mass is about 460 kg. This also defines the type of rocket that is suitable for the mission. (4) The cost of the launch. A cheaper cost makes the mission more feasible.

Combining the above considerations, the circular orbit is not the best option. Here we propose a low cost scheme (a more detailed and complete analysis of the mission profile and design can be found in the companion paper [27]). The elliptical orbit with the perihelion between 0.7 and 0.85 AU and the aphelion at 1 AU (Figure 8) is preliminarily adopted. In this scheme, one rocket two spacecraft technology could be applied to shorten the deployment time and save the launch cost. But a few fuel is needed for the second spacecraft to adjust the orbital phase to accomplish the 30° separation from the first spacecraft. The time for the orbital phase adjustment is about one year, but really depending on the perihelion and the carrying capacity of the rocket. The preferred rocket could be Long March 3A (LM-3A), which has the carrying capacity of about 1400 kg and can carry two spacecraft each time. To make an even faster deployment, Long March 3B (LM-3B), which has much larger carry capacity, could be considered, but the cost is about two times of that of using LM-3A.

If choosing the elliptical orbit with the perihelion of 0.85

AU, the spacecraft separate from the Earth at a speed of about 47° per year. After 2.54 years, the second group of spacecraft could be launched to form 120° separation between the two groups. Similarly, the third group will be launched about 5.08 years later since the launch of the first group. The final configuration of the Solar Ring will form in about 6.5 years. A smaller perihelion could be chosen to shorten the deployment time. If the perihelion, for example, is 0.7 AU, the total time to finish the deployment is about 3.65 years, but the carrying capacity of LM-3A may not be sufficient. Besides, it should be noted that the three groups of the spacecraft are not on the same elliptical orbit in this launch scheme (Figure 8), and therefore the separation angles among them will vary around the designed values with time. This is acceptable as our science objectives do not require the fixed separation angles and heliocentric distances of the spacecraft.

In this design, the distance between the spacecraft and Earth varies within 2 AU. A larger antenna and power is required to receive sufficient data. Assuming each spacecraft is equipped a communication antenna with the aperture of 1.2 m and supplied with the power of 70 W, we have the data transmission rate from about 5000 kbps at 0.25 AU away from the Earth to less than 70 kbps at 2 AU away by using the 66-m telescope at Jiamusi station (see Figure 9). If we have 8 h for data transmission every day, we can receive less than 20 GB data per day at 0.25 AU away or 200 MB per day at 2 AU away for one spacecraft. It is much lower than the desired data rate based on the current payload requirement, becoming the the strongest restriction to this mission. To solve or relieve this problem, either we reduce the data rate by
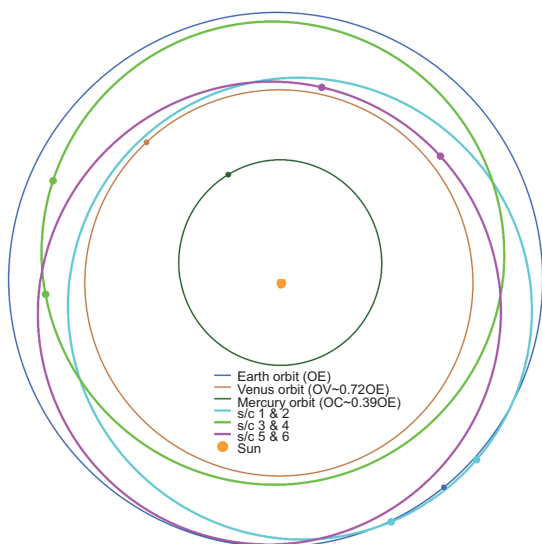

Figure 9   The data transmission rate as a function of the distance between the spacecraft and Earth. Different lines show the rate for the telescope with different size and different power.

enhancing the capability of the onboard data processing, compression and storage and decreasing the sampling frequency, or we develop more efficient techniques for the deep space communication, e.g., laser communication [101].

5   Summary and conclusions

This ambitious concept of Solar Ring mission aims to achieve unprecedented capabilities to advance our understanding of the Sun and the inner heliosphere from four aspects: the origin of solar cycle, the origin of solar eruptions, the origin of solar wind structures and the origin of severe space weather events. The cost of the whole mission is huge, but the design of the three groups of spacecraft makes the international collaboration being an option, which may reduce the financial load of any single country. There are lots of challenges in the technique of carrier, control, communication, payloads, etc, that need to be justified in the next study. We are looking forward to the mission concept coming true.

Figure 8   The elliptical orbits (cyan, light green and pink) of the three groups of the spacecraft with the perihelion of 0.75 AU and the aphelion of 1 AU. In this scheme, the separation angle among the three groups oscillates around 120° and the angle between the spacecraft in each group oscillates around 30°.
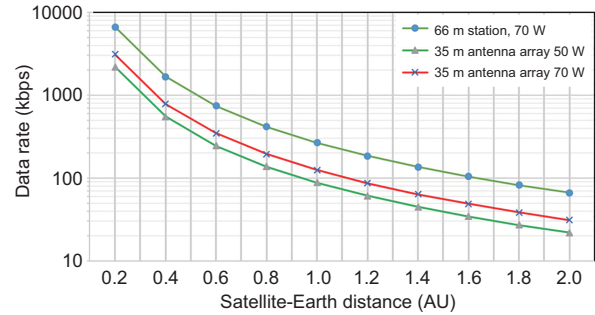
1   Hudson H S, Bougeret J L, Burkepile J. Coronal mass ejections: Overview of observations. Space Sci Rev, 2006, 123: 13–30

2   Yashiro S. A catalog of white light coronal mass ejections observed by the SOHO spacecraft. J Geophys Res, 2004, 109: A07105

3   Dikpati M, Charbonneau P. A babcock-leighton flux transport dynamo with solar-like differential rotation. Astrophys J, 1999, 518: 508–520

4   Reid G C. Solar variability and its implications for the human environment. J Atmos Sol-Terrestrial Phys, 1999, 61: 3–14

5   Lean J, Rind D. Evaluating sun-climate relationships since the little ice age. J Atmos Sol-Terrestrial Phys, 1999, 61: 25–36

6   Nandy D, Muñoz-Jaramillo A, Martens P C H. The unusual minimum of sunspot cycle 23 caused by meridional plasma flow variations. Nature, 2011, 471: 80–82

7   Schrijver C J, Livingston W C, Woods T N, et al. The minimal solar activity in 2008–2009 and its implications for long-term climate modeling. Geophys Res Lett, 2011, 38: L06701

8   McComas D J, Angold N, Elliott H A, et al. Weakest Solar wind of the space age and the current "mini" solar maximum. Astrophys J, 2013, 779: 2

9   Feulner G, Rahmstorf S. On the effect of a new grand minimum of solar activity on the future climate on Earth. Geophys Res Lett, 2010, 37: L05707

10 Domingo V, Fleck B, Poland A I. SOHO: The solar and heliospheric observatory. Space Sci Rev, 1995, 72: 81–84

11 Handy B N, Acton L W, Kankelborg C C, et al. The transition region and coronal explorer. Sol Phys, 1999, 187: 229–260

12 Ogawara Y, Takano T, Kato T, et al. The solar-A mission—An overview. Sol Phys, 1991, 136: 1–16

13 Pesnell W D, Thompson B J, Chamberlin P C. The solar dynamics observatory (SDO). Sol Phys, 2012, 275: 3–15

14 Kosugi T, Matsuzaki K, Sakao T, et al. The hinode (solar-B) mission: An overview. Sol Phys, 2007, 243: 3–17

15 Kaiser M L, Kucera T A, Davila J M, et al. The stereo mission: An introduction. Space Sci Rev, 2008, 136: 5–16

16 Müller D, Marsden R G, St. Cyr O C, et al. Solar orbiter. Exploring the sun-heliosphere connection. Sol Phys, 2013, 285: 25–70

17 Ogilvie K W, Parks G K. First results from WIND spacecraft: An introduction. Geophys Res Lett, 1996, 23: 1179–1181

18 Stone R G, Frandsen A M, Mewaldt R A, et al. The advanced composition explorer. Space Sci Rev, 1998, 86: 1–22

19 NOAA. Dscovr: Deep space climate observatory. 2015. https://www.nesdis.noaa.gov/content/dscovr-deep-space-climate-observatory

20 Winkler W. HELIOS assessment and mission results. Acta Astronaut, 1976, 3: 435–447

21 Wenzel K P, Marsden R G, Page D E, et al. The Ulysses mission. Astron Astrophys Suppl, 1992, 92: 207

22 Fox N J, Velli M C, Bale S D, et al. The solar probe plus mission: Humanity's first visit to our star. Space Sci Rev, 2016, 204: 7–48

23 Solomon S C, McNutt Jr. R L, Gold R E, et al. MESSENGER mission overview. Space Sci Rev, 2007, 131: 3–39

24 Svedhem H, Titov D V, McCoy D, et al. Venus expressⅼthe first european mission to venus. Planet Space Sci, 2007, 55: 1636–1652

25 Schmidt R. Mars express-ESA's first mission to planet Mars. Acta Astronaut, 2003, 52: 197–202

26 Jakosky B M, Lin R P, Grebowsky J M, et al. The mars atmosphere and volatile evolution (MAVEN) mission. Space Sci Rev, 2015, 195: 3–48

27 Wang Y M, Chen X, Wang P C, et al. Concept of the solar ring mission: Preliminary design and mission profile. Sci China Tech Sci, 2020, doi: 10.1007/s11431-020-1612-y

28 Allen Gary G, Hagyard M J. Transformation of vector magnetograms and the problems associated with the effects of perspective and the azimuthal ambiguity. Sol Phys, 1990, 126: 21–36

29 Schou J, Scherrer P H, Bush R I, et al. Design and ground calibration of the helioseismic and magnetic imager (HMI) instrument on the solar dynamics observatory (SDO). Sol Phys, 2012, 275: 229–259

30 Liu L, Wang Y, Wang J, et al. Why is a flare-rich active region CME-poor? Astrophys J, 2016, 826: 119

31 Jin C L, Wang J X, Xie Z X. Solar intranetwork magnetic elements: Intrinsically weak or strong? Sol Phys, 2012, 280: 51–67

32 Wiegelmann T, Sakurai T. Solar force-free magnetic fields. Living Rev Sol Phys, 2012, 9: 5

33 Wiegelmann T. Nonlinear force-free modeling of the solar coronal magnetic field. J Geophys Res, 2008, 113: A03S02

34 Christensen-Dalsgaard J, Dappen W, Ajukov S V, et al. The current state of solar modeling. Science, 1996, 272: 1286–1292

35 Scherrer P H, Bogart R S, Bush R I, et al. The solar oscillations investigation-michelson doppler imager. Sol Phys, 1995, 162: 129–188

36 Harvey J W, Hill F, Hubbard R P, et al. The global oscillation network group (GONG) project. Science, 1996, 272: 1284–1286

37 Thompson M J, Toomre J, Anderson E R, et al. Differential rotation and dynamics of the solar interior. Science, 1996, 272: 1300–1305

38 Howe R, Christensen-Dalsgaard J, Hill F, et al. Deeply penetrating banded zonal flows in the solar convection zone. Astrophys J, 2000, 533: L163–L166

39 Zhao J, Bogart R S, Kosovichev A G, et al. Detection of equatorward meridional flow and evidence of double-cell meridional circulation inside the sun. Astrophys J, 2013, 774: L29

40 Miesch M S, Brown B P. Convective babcock-leighton dynamo models. Astrophys J, 2012, 746: L26

41 Simnett G M, Hudson H S. The evolution of a rapidly-expanding active region loop into a trans-equatorial coronal mass ejection. In: Prcoceedings of the Correlated Phenomena at the Sun, in the Heliosphere and in Geospace, 31st ESLAB symposium (ESA SP-415). Netherlands, 1997. 437–441

42 Moon Y J, Choe G S, Wang H, et al. Sympathetic coronal mass ejections. Astrophys J, 2003, 588: 1176–1182

43 Zhou G, Wang J, Wang Y, et al. Quasi-simultaneous flux emergence in the events of October–November 2003. Sol Phys, 2007, 244: 13–24

44 Schrijver C J, Title A M. Long-range magnetic couplings between solar flares and coronal mass ejections observed by SDO and STEREO. J Geophys Res, 2011, 116: A04108

45 Zhang Y, Wang J, Attrill G D R, et al. Coronal magnetic connectivity and EUV dimmings. Sol Phys, 2007, 241: 329–349

46 Pevtsov A A. Transequatorial loops in the solar corona. Astrophys J, 2000, 531: 553–560

47 Heinemann S G, Temmer M, Hofmeister S J, et al. Three-phase evolution of a coronal hole. I. 360° remote sensing and *in situ* observations. Astrophys J, 2018, 861: 151

48 Liu Y, Hoeksema J T, Scherrer P H, et al. Comparison of line-of-sight magnetograms taken by the solar dynamics observatory/helioseismic and magnetic imager and solar and heliospheric observatory/michelson doppler imager. Sol Phys, 2012, 279: 295–316

49 Aschwanden M J, Wülser J P, Nitta N V, et al. First three-dimensional reconstructions of coronal loops with the STEREO A and B spacecraft. I. Geometry. Astrophys J, 2008, 679: 827–842

50 Liu J J, Wang Y M, Liu R, et al. When and how does a prominence-like jet gain kinetic energy? Astrophys J, 2014, 782: 94

51 Kwon R Y, Chae J, Zhang J. Stereoscopic determination of heights of extreme ultraviolet bright points using data taken by SECCHI/EUVI aboard STEREO. Astrophys J, 2010, 714: 130–137

52 Robbrecht E, Patsourakos S, Vourlidas A. No trace left behind: STEREO observation of a coronal mass ejection without low coronal signatures. Astrophys J, 2009, 701: 283–291

53 Wang Y, Chen C, Gui B, et al. Statistical study of coronal mass ejection source locations: Understanding CMEs viewed in coronagraphs. J Geophys Res, 2011, 116: A04104

54 Thernisien A F R, Howard R A, Vourlidas A. Modeling of flux rope coronal mass ejections. Astrophys J, 2006, 652: 763–773

55 Sheeley N R, Lee D D H, Casto K P, et al. The structure of streamer blobs. Astrophys J, 2009, 694: 1471–1480

56 Lugaz N, Vourlidas A, Roussev I I. Deriving the radial distances of wide coronal mass ejections from elongation measurements in the heliosphere—application to CME-CME interaction. Ann Geophys, 2009, 27: 3479–3488

57 Feng L, Inhester B, Mierla M. Comparisons of CME morphological characteristics derived from five 3D reconstruction methods. Sol Phys, 2013, 282: 221–238

58 Li X L, Wang Y M, Liu R, et al. Reconstructing solar wind inhomogeneous structures from stereoscopic observations in white-light: Solar wind transients in 3d. J Geophys Res Space Phys, 2020, doi: 10.1029/2019JA027513

59 Li X L, Wang Y M, Liu R, et al. Reconstructing solar wind inhomogeneous structures from stereoscopic observations in white-light: Small transients along the Sun-Earth line. J Geophys Res Space Phys, 2018, 123: 7257–7270

60 Wang Y, Zhang Q, Liu J, et al. On the propagation of a geoeffective coronal mass ejection during 15–17 March 2015. J Geophys Res Space Phys, 2016, 121: 7423–7434

61 Wang Y, Shen C, Wang S, et al. Deflection of coronal mass ejection in the interplanetary medium. Sol Phys, 2004, 222: 329–343

62 Riley P, Crooker N U. Kinematic treatment of coronal mass ejection evolution in the solar wind. Astrophys J, 2004, 600: 1035–1042

63 Manchester IV W, Gombosi T, DeZeeuw D, et al. Eruption of a buoyantly emerging magnetic flux rope. Astrophys J, 2004, 610: 588–596

64 Wang Y, Wang B, Shen C, et al. Deflected propagation of a coronal mass ejection from the corona to interplanetary space. J Geophys Res Space Phys, 2014, 119: 5117–5132

65 Kay C, Opher M. The heliocentric distance where the deflections and rotations of solar coronal mass ejections occur. Astrophys J, 2015, 811: L36

66 Gopalswamy N, Lara A, Lepping R P, et al. Interplanetary acceleration of coronal mass ejections. Geophys Res Lett, 2000, 27: 145–148

67 Vršnak B, Vrbanec D, Čalogović J. Dynamics of coronal mass ejections. Astron Astrophys, 2008, 490: 811–815

68 Vršnak B, Žic T, Vrbanec D, et al. Propagation of interplanetary coronal mass ejections: The drag-based model. Sol Phys, 2013, 285: 295–315

69 Shen C L, Wang Y M, Pan Z H, et al. Full-halo coronal mass ejections: Arrival at the Earth. J Geophys Res Space Phys, 2014, 119: 5107–5116

70 Dasso S, Mandrini C H, Démoulin P, et al. A new model-independent method to compute magnetic helicity in magnetic clouds. Astron Astrophys, 2006, 455: 349–359

71 Ruffenach A, Lavraud B, Farrugia C J, et al. Statistical study of magnetic cloud erosion by magnetic reconnection. J Geophys Res Space Phys, 2015, 120: 43–60

72 Wang Y M, Shen C L, Liu R, et al. Understanding the twist distribution inside magnetic flux ropes by anatomizing an interplanetary magnetic cloud. J Geophys Res Space Phys, 2018, 123: 3238–3261

73 Shen C, Wang Y, Wang S, et al. Super-elastic collision of large-scale magnetized plasmoids in the heliosphere. Nat Phys, 2012, 8: 923–928

74   Lugaz N, Farrugia C J, Davies J A, et al. The deflection of the two interacting coronal mass ejections of 2010 May 23–24 as revealed by combined in site measurements and heliospheric imaging. Astrophys J, 2012, 759: 68

75 Temmer M, Veronig A M, Peinhart V, et al. Asymmetry in the CME-CME interaction process for the events from 2011 February 14–15. Astrophys J, 2014, 785: 85

76 Mishra W, Wang Y, Srivastava N, et al. Assessing the nature of collisions of coronal mass ejections in the inner heliosphere. Astrophys J Suppl Ser, 2017, 232: 5

77 Larson D E, Lin R P, McTiernan J M, et al. Tracing the topology of the October 18–20, 1995, magnetic cloud with ∼ $0.1 - 10^2$ kev electrons. Geophys Res Lett, 1997, 24: 1911–1914

78 Wang Y, Zhou Z, Shen C, et al. Investigating plasma motion of magnetic clouds at 1 AU through a velocity-modified cylindrical force-free flux rope model. J Geophys Res Space Phys, 2015, 120: 1543–1565

79 Wang Y, Zhuang B, Hu Q, et al. On the twists of interplanetary magnetic flux ropes observed at 1 AU. J Geophys Res Space Phys, 2016, 121: 9316–9339

80 Démoulin P, Janvier M, Dasso S. Magnetic flux and helicity of magnetic clouds. Sol Phys, 2016, 291: 531–557

81 Owens M J. Do the legs of magnetic clouds contain twisted flux-rope magnetic fields? Astrophys J, 2016, 818: 197

82 Zhao A, Wang Y, Chi Y, et al. Main cause of the poloidal plasma motion inside a magnetic cloud inferred from multiple-spacecraft observations. Sol Phys, 2017, 292: 58

83 Owens M J, Lockwood M, Barnard L A. Coronal mass ejections are not coherent magnetohydrodynamic structures. Sci Rep, 2017, 7: 4152

84 Desai M, Giacalone J. Large gradual solar energetic particle events. Living Rev Sol Phys, 2016, 13: 3

85 Cane H V, Reames D V, von Rosenvinge T T. The role of interplanetary shocks in the longitude distribution of solar energetic particles. J Geophys Res, 1988, 93: 9555–9567

86 Guo J N, Dumbović M, Wimmer-Schweingruber R F, et al. Modeling the evolution and propagation of 10 September 2017 CMEs and SEPs arriving at Mars constrained by remote sensing and *in situ* measurement. Space Weather, 2018, 16: 1156–1169

87 Hassler D M, Zeitlin C, Wimmer-Schweingruber R F, et al. The radiation assessment detector (RAD) investigation. Space Sci Rev, 2012, 170: 503–558

88 Wang Y, Zhang J, Shen C. An analytical model probing the internal state of coronal mass ejections based on observations of their expansions and propagations. J Geophys Res, 2009, 114: A10104

89 Mishra W, Wang Y. Modeling the thermodynamic evolution of coronal mass ejections using their kinematics. Astrophys J, 2018, 865: 50

90 Wang Y, Cao H, Chen J, et al. Solar limb prominence catcher and tracker (SLIPCAT): An automated system and its preliminary statistical results. Astrophys J, 2010, 717: 973–986

91 Gosling J T. Magnetic reconnection in the solar wind. Space Sci Rev, 2012, 172: 187–200

92 Shen F, Shen C, Wang Y, et al. Could the collision of CMEs in the heliosphere be super-elastic? Validation through three-dimensional simulations. Geophys Res Lett, 2013, 40: 1457–1461

93 Reiner M J, Stone R G. A new method for reconstructing Type-III trajectories. Sol Phys, 1986, 106: 397–401

94 Krupar V, Maksimovic M, Santolik O, et al. Statistical survey of type III radio bursts at long wavelengths observed by the solar terrestrial relations observatory (STEREO)/waves instruments: Goniopolarimetric properties and radio source locations. Sol Phys, 2014, 289: 4633–4652

95   Magdalenić J, Marqué C, Krupar V, et al. Tracking the CME-driven shock wave on 2012 March 5 and radio triangulation of associated radio emission. Astrophys J, 2014, 791: 115

96 Zhang P, Wang C, Ye L, et al. Forward modeling of the type III radio burst exciter. Sol Phys, 2019, 294: 62

97 Cecconi B, Bonnin X, Hoang S, et al. STEREO/waves goniopolarimetry. Space Sci Rev, 2008, 136: 549–563

98 Leamon R J, Smith C W, Ness N F, et al. Observational constraints on the dynamics of the interplanetary magnetic field dissipation range. J Geophys Res, 1998, 103: 4775–4788

99 Hu R X, Shan X, Yuan G Y, et al. A low-energy ion spectrometer with half-space entrance for three-axis stabilized spacecraft. Sci China Tech Sci, 2019, 62: 1015–1027

100 Malandraki O E, Lario D, Lanzerotti L J, et al. October/November 2003 interplanetary coronal mass ejections: ACE/EPAM solar energetic particle observations. J Geophys Res, 2005, 110: A09S06

101 Wu W, Chen M, Zhang Z, et al. Overview of deep space laser communication. Sci China Inf Sci, 2018, 61: 040301